

# Semantics Prompting Data-Free Quantization for Low-Bit Vision Transformers

Yunshan Zhong<sup>1,2</sup>, Yuyao Zhou<sup>2</sup>, Yuxin Zhang<sup>2</sup>, Shen Li<sup>3</sup>, Yong Li<sup>3</sup>,  
Fei Chao<sup>2</sup>, Zhanpeng Zeng<sup>2</sup>, Rongrong Ji<sup>1,2\*</sup>

<sup>1</sup>Institute of Artificial Intelligence, Xiamen University

<sup>2</sup>MAC Lab, Department of Artificial Intelligence, School of Informatics, Xiamen University

<sup>3</sup>Alibaba

zhongyunshan@stu.xmu.edu.cn, jiawei.hu@stu.xmu.edu.cn

linmb001@outlook.com, cmzxmu@stu.xmu.edu.cn, rrji@xmu.edu.cn

## Abstract

*Data-free quantization (DFQ), which facilitates model quantization without real data to address increasing concerns about data security, has garnered significant attention within the model compression community. Recently, the unique architecture of vision transformers (ViTs) has driven the development of specialized DFQ techniques. However, we observe that the synthetic images from existing methods suffer from the deficient semantics issue compared to real images, thereby compromising performance. Motivated by this, we propose SPDFQ, a Semantics Prompting Data-Free Quantization method for ViTs. First, SPDFQ incorporates Attention Priors Alignment (APA), which uses randomly generated attention priors to enhance the semantics of synthetic images. Second, SPDFQ introduces Multi-Semantic Reinforcement (MSR), which utilizes localized patch optimization to prompt efficient parameterization and diverse semantics in synthetic images. Finally, SPDFQ employs Softlabel Learning (SL), where soft learning targets are adapted to encourage more complex semantics and accommodate images augmented by MSR. Experimental results demonstrate that SPDFQ significantly outperforms existing methods. For instance, SPDFQ achieves a 15.52% increase in top-1 accuracy on ImageNet for W4A4 ViT-B<sup>1</sup>.*

## 1. Introduction

Vision transformers (ViTs) [19] have attracted widespread interest from both academia and industry [26, 33] due to their superior performance across various vision tasks [1, 7, 52, 62]. However, the substantial computational demands and high memory requirements of ViTs pose significant challenges for deployment in resource-limited environ-

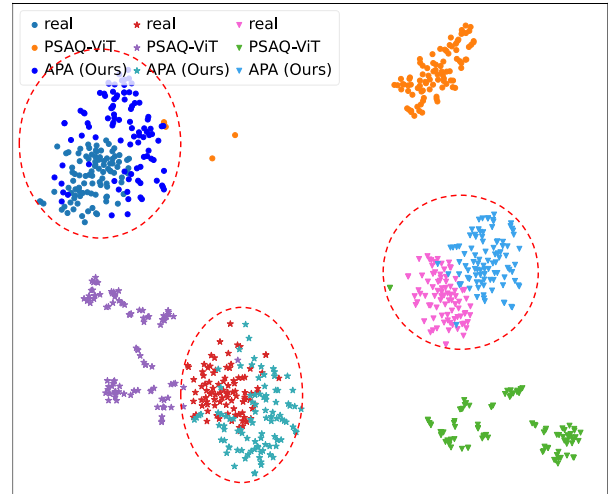


Figure 1. Feature visualization using  $t$ -SNE [63]. Each shape (circle, star, triangle) represents a category. The red dashed circles highlight the features of our APA and real images. The visualized features are activations extracted before the classification head of DeiT-S. The features from PSAQ-ViT [43] deviate significantly from those of the real images, suggesting deficient semantics. While the features from our APA are more closely aligned with those of real images, suggesting improved semantics.

ments [11, 27, 29, 42, 51, 61, 75]. To address this challenge, model quantization [36] has emerged as a promising solution, reducing model complexity by enabling a low-bit representation of weights and activations. Nevertheless, most existing quantization methods rely on access to the original training data, raising concerns regarding data privacy and security. This data dependency restricts their application in data-sensitive environments [6, 24, 70, 77].

To address this limitation, data-free quantization (DFQ) has been developed to quantize models without accessing real data, attracting considerable attention [14, 69, 74].

\*Corresponding Author: rrji@xmu.edu.cn

<sup>1</sup>The code will be made publicly available upon acceptance.

Most existing DFQ methods are tailored to convolutional neural networks (CNNs) and are not directly applicable to ViTs. These methods typically utilize batch normalization statistics (BNS), which capture the distribution of real data, to synthesize in-distribution synthetic data [6, 69, 74, 77]. However, BNS is unavailable for ViTs that use layer normalization (LN) to dynamically compute distribution statistics during inference [43]. Recently, several works have been proposed to accommodate the unique structure of ViTs [16, 30, 43, 44, 58]. For example, PSAQ-ViT [43] introduces patch similarity entropy (PSE) loss to optimize Gaussian noise towards usable synthetic images.

Nevertheless, we observe that the current synthetic images suffer from the deficient semantics issue. In Fig. 1, we visualize the penultimate features of the synthetic images using t-SNE [63]. It can be observed that the features of synthetic images generated by PSAQ-ViT diverge significantly from those of real images, suggesting that these synthetic images are semantically deficient. This observation is further supported by the quantitative results in Tab. 1, where the cosine similarity between synthetic images from PSAQ-ViT and real images is notably low. For high-bit quantization, where model capacity is largely retained [39], the performance degradation remains relatively minor even with deficient semantics images [43, 58]. However, in low-bit quantization, where model capacity is severely damaged and informative images are essential for recovering performance [13, 77], fine-tuning on these deficient semantics images leads to poor generalization to real datasets, resulting in limited performance gains.

Motivated by this finding, we propose a **Semantics Prompting Data-Free Quantization** method for ViTs, termed SPDFQ. The overall framework is depicted in Fig. 2. First, SPDFQ introduces Attention Priors Alignment (APA), which employs randomly generated priors to encourage high responses in attention maps, thereby explicitly promoting semantics in synthetic images. These priors are generated using the Gaussian Mixture Model (GMM) to simulate diverse attention patterns. APA effectively prompts semantics in synthetic images, as validated by both visualization and quantitative analyses. As shown in Fig. 1, features of APA exhibit a closer alignment to those of real images, indicating high semantics. The quantitative results in Tab. 1 further confirm that the semantics of APA are more similar to the real images. Additionally, SPDFQ incorporates Multi-Semantic Reinforcement (MSR) and Softlabel Learning (SL). MSR promotes efficient parameterization and diverse semantics in synthetic images by leveraging localized patch-wise optimization, while SL prompts more complex semantics in synthetic images and accommodates images augmented by MSR through the use of soft learning targets.

Experimental results across various ViT models demon-

strate that SPDFQ presents substantial performance improvements. For example, SPDFQ achieves a 15.52% increase in top-1 accuracy on the ImageNet dataset for the W4A4 ViT-B model.

## 2. Related Works

### 2.1. Vision Transformers

The great success of transformers in the natural language processing field has driven widespread attempts in the computer vision community to apply them to vision tasks [12, 25, 65]. ViT [19] is the pioneer that builds a transformer-based model to handle images, boosting the performance on the image classification task. DeiT [62] introduces an efficient teacher-student training strategy where a distillation token is employed to distill knowledge from the teacher model to the student model. Swin Transformers [50] builds an efficient and effective hierarchical model by introducing a shifted window-based self-attention mechanism. Other than the image classification task, the applications of ViTs also have broadened considerably, manifesting groundbreaking performance in object detection [7], image segmentation [9, 76], low-level vision [46], video recognition [1, 55], and medical image processing [60], *etc.* Nevertheless, the impressive performance of ViTs relies on a high number of parameters and significant computational overhead, preventing deployment in resource-constrained environments. Several recent efforts design lightweight ViTs, such as MobileViT [53], MiniViT [73], and TinyViT [66]. However, the model complexity is still unsatisfactory [43].

### 2.2. Network Quantization

**Data-Driven Quantization.** Model quantization reduces the complexity of neural networks by replacing full-precision weight and activation with the low-bit format. Data-driven quantization can be roughly divided into two categories: quantization-aware training (QAT) and post-training quantization (PTQ). QAT is compute-heavy since it re-trains the quantized model with the full training data to retain performance [20, 22, 38, 40, 42, 48, 67]. PTQ perform quantization with a tiny dataset and a reduced time overhead, harvesting widespread attention [3, 39]. The specific architecture of ViTs, such as LayerNorm and the self-attention module, urges distinct PTQ methods compared to CNNs [18, 21, 42, 47, 49, 79]. For example, Liu *et al.* [51] develop a ranking loss to maintain the relative order of the self-attention activation. Unfortunately, both QAT and PTQ involve the original training data, causing concerns about data privacy and security issues in data-sensitive scenarios.

**Data-Free Quantization.** DFQ quantizes models without accessing real data [2, 13–15, 24, 32, 37, 41, 57]. Most previous DFQ methods focus on CNN, where the BNS can be adopted as the regularization term [6, 74]. How-

ever, BNS is infeasible for ViTs built on the LN. Recently, few efforts have been explored to accommodate ViTs [16, 30, 43, 44, 58]. PSAQ-ViT [43] introduces the first DFQ method for ViTs. They discover that Gaussian noise yields homogeneous patches, while the real image yields heterogeneous patches. Thus, patch similarity entropy (PSE) loss is proposed to optimize the Gaussian noise towards real-like images by making them showcase heterogeneous patches. Based on PSAQ-ViT, PSAQ-ViT V2 [44] further introduces an adversarial learning strategy [23]. [58] incorporates contrastive learning and proposes an iterative generation-quantization PTQ-based DFQ method. [30] proposes a sparse generation method to remove noisy and hallucination backgrounds in synthetic images.

### 3. Method

#### 3.1. Preliminaries

##### 3.1.1. Quantizers

We employ the linear quantizer for all weights and activations, except for the attention scores, which use a log2 quantizer to handle highly non-negative and uneven values [21, 45, 47]. For the linear quantizer, given a full-precision input  $\mathbf{x}$  and bit-width  $b$ , the quantized value  $\mathbf{x}_q$  and the de-quantized value  $\bar{\mathbf{x}}$  are computed as follows:

$$\mathbf{x}_q = \text{clip} \left( \left\lfloor \frac{\mathbf{x}}{\Delta} \right\rfloor + z, 0, 2^b - 1 \right), \bar{\mathbf{x}} = \Delta \cdot (\mathbf{x}_q - z), \quad (1)$$

where  $\lfloor \cdot \rfloor$  denotes rounding to the nearest integer, and clip limits the value to  $[0, 2^b - 1]$ . Here,  $\Delta$  and  $z$  are the scale factor and zero-point, respectively. For the log2 quantizer:

$$\mathbf{x}_q = \text{clip} \left( \left\lfloor -\log_2 \frac{\mathbf{x}}{\Delta} \right\rfloor, 0, 2^b - 1 \right), \bar{\mathbf{x}} = \Delta \cdot 2^{-\mathbf{x}_q}. \quad (2)$$

##### 3.1.2. Data Synthesis

DFQ methods parameterize synthetic images and optimize them toward real-like images with a pre-trained full-precision model  $F$ . Given an image  $\tilde{\mathbf{I}}$  initialized from Gaussian noise, the one-hot loss [68] is introduced to prompt label-related semantics:

$$\mathcal{L}^{\text{OH}}(\tilde{\mathbf{I}}) = CE(F(\tilde{\mathbf{I}}), c) \quad (3)$$

where  $CE(\cdot, \cdot)$  represents the cross entropy,  $c$  is a random class label, and  $F(\cdot)$  returns the predicted probability for image  $\tilde{\mathbf{I}}$ .

Moreover, total variance (TV) [70] loss is a smoothing regularization term to improve the image quality:

$$\mathcal{L}^{\text{TV}}(\tilde{\mathbf{I}}) = \iint |\nabla \tilde{\mathbf{I}}(\tau_1, \tau_2)| d\tau_1 d\tau_2. \quad (4)$$

where  $\nabla \tilde{\mathbf{I}}(\tau_1, \tau_2)$  denotes the gradient at  $\tilde{\mathbf{I}}$  at  $(\tau_1, \tau_2)$ .

To perform DFQ for ViTs, PSAQ-ViT [43] proposes patch similarity entropy (PSE) loss. It first computes patch similarity  $\Gamma_l[i, j] = \frac{u_i \cdot u_j}{\|u_i\| \|u_j\|}$ , where  $u_i, u_j$  are feature vectors of MHA outputs in  $l$ -th block and  $\|\cdot\|$  denotes the  $l_2$  norm. Then, it estimates the density function  $\hat{f}_l(x) = \frac{1}{Mh} \sum_{m=1}^M K\left(\frac{x-x_m}{h}\right)$ , where  $K(\cdot)$  is a normal kernel,  $h$  is the bandwidth, and  $x_m$  is the kernel center derived from  $\Gamma_l$ . Finally, the PSE loss is defined as:

$$\mathcal{L}^{\text{PSE}}(\tilde{\mathbf{I}}) = \sum_{l=1}^L \int \hat{f}_l(x) \log[\hat{f}_l(x)] dx, \quad (5)$$

where  $L$  is the block number of the model.

#### 3.2. Observations

Although existing DFQ methods of ViTs have made some progress, a significant performance gap remains between synthetic and real images. For example, as shown in Tab. 2, the W4A4 ViT-B fine-tuned on real images yields 68.16%, whereas PSAQ-ViT only achieves 36.32%. To dive into a deeper analysis, we visualize the features of the synthetic images before the classification head using t-SNE [63] in Fig. 1. Generally, the penultimate feature represents the semantics of the input [4, 54, 71, 72].

It is evident that features of PSAQ-ViT diverge significantly from those of real samples, indicating that the synthetic images fail to capture the real semantics distribution. We refer to this phenomenon as the deficient semantics issue. In Tab. 1, we quantitatively measure the semantics using the average cosine similarity (ranging from  $-1$  to  $1$ ). We also report the intra-class similarity within real images as an approximate upper bound for comparison. These results further highlight the deficient semantics of PSAQ-ViT. For example, for Class 1, the intra-class similarity within real images is 0.68, whereas PSAQ-ViT only presents 0.44, suggesting a low similarity between synthetic and real images. Similarly, for Class 3, while the real images exhibit a similarity of 0.41, PSAQ-ViT achieves only 0.31.

Both visualization and quantitative results reveal a pronounced deficient semantics. Consequently, quantized models fine-tuned on these semantically deficient synthetic images cannot well generalize to the real dataset, resulting in limited performance.

#### 3.3. Solutions

In the following, we introduce the proposed SPDFQ to prompt semantics in synthetic images. As illustrated in Fig. 2, SPDFQ introduces three contributions: Attention Priors Alignment (APA), Multi-Semantic Reinforcement (MSR), and Softlabel Learning (SL).

##### 3.3.1. Attention Priors Alignment

The first step of SPDFQ in prompting semantics leverages the self-attention mechanism of ViTs. Specifically, the self-

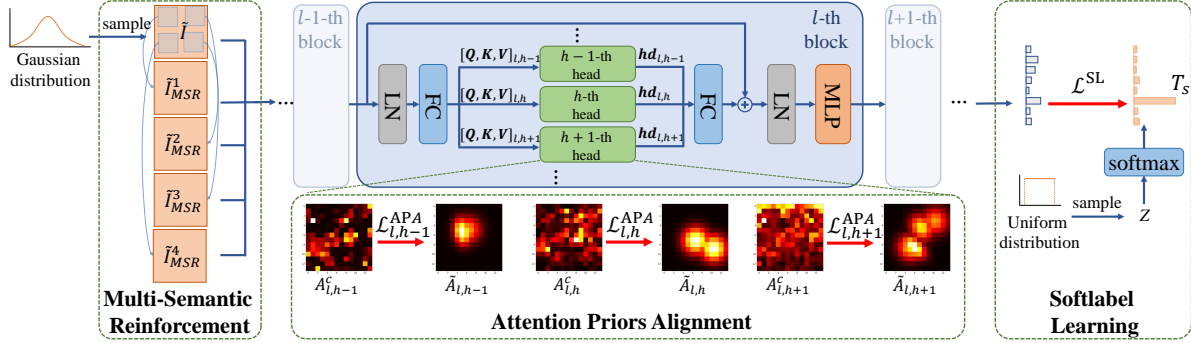


Figure 2. Framework of the proposed SPDFQ. Attention Priors Alignment (APA) employs randomly generated attention priors to explicitly promote semantics in synthetic images. Multi-Semantic Reinforcement (MSR) prompts the different parts of synthetic images with various semantics. Softlabel Learning (SL) leverages soft learning to prompt more complex semantics in synthetic images.

Classes \ Method	Real	PSAQ-ViT [43]	APA (Ours)
Class 1	0.68	0.44	0.64
Class 2	0.32	0.26	0.31
Class 3	0.41	0.31	0.36

Table 1. Average cosine similarity of three randomly selected classes. For real images, the similarity is measured within the class itself, while for PSAQ-ViT and APA, the similarity is measured between synthetic and real images of the same class. The results show that APA achieves higher similarity than PSE loss, indicating improved semantics.

attention mechanism extracts and integrates semantic information by allocating more attention to tokens rich in semantics and less to tokens with minimal semantics [10, 19, 28]. Thus, if a synthetic image is semantically rich, its attention maps should exhibit high responses. Based on this characteristic, we propose Attention Priors Alignment (APA), which is designed to promote the semantics of synthetic images by explicitly encouraging high responses in images’ attention maps.

For a synthetic image  $\tilde{I}$ , we first extract its attention maps of the  $h$ -th head in the  $l$ -th block, denoted by  $\mathbf{A}_{l,h} \in \mathbb{R}^{N \times N}$ , by inputting the image into a pre-trained full-precision model, where  $N$  represents the total number of tokens. In DeiT, the attention of the classification token toward other tokens serves as the indicator for semantic versus non-semantic parts [5]. Accordingly, we extract  $\mathbf{A}_{l,h}^c \in \mathbb{R}^{1 \times (N-1)}$  from  $\mathbf{A}_{l,h}$ , representing the attention of the classification token to all tokens except itself. We then randomly generate attention priors  $\tilde{\mathbf{A}}_{l,h}$ , whose generation is detailed in the next part, and align  $\mathbf{A}_{l,h}^c$  with  $\tilde{\mathbf{A}}_{l,h}$  by:

$$\mathcal{L}_{l,h}(\tilde{I}) = \text{MSE}(\mathbf{A}_{l,h}^c - \tilde{\mathbf{A}}_{l,h}), \quad (6)$$

where MSE represents the mean squared error. For Swin

models that do not use a classification token, we substitute  $\mathbf{A}_{l,h}^c$  in Eq. 6 with the average attention map of all tokens [10]. As noted in [17], ViTs initially focus on all regions to capture low-level information in shallow blocks and gradually shift their focus toward semantic regions in deeper blocks to extract high-level semantic information. Leveraging this property, we selectively apply  $\mathcal{L}_{l,h}^{\text{APA}}$  to deeper blocks, progressively aligning attention towards semantically relevant areas. The total APA loss is computed as a depth-weighted sum of the individual Eq. 6 across these deeper blocks:

$$\mathcal{L}^{\text{APA}}(\tilde{I}) = \sum_{l=S}^L \sum_{h=1}^H \frac{l}{L} \mathcal{L}_{l,h}(\tilde{I}), \quad (7)$$

where  $S$  is a pre-given hyper-parameter denoting the start of deep blocks and are experimentally set  $S = \frac{L}{2}$ .

The proposed APA loss encourages synthetic images to contain semantically meaningful regions with high responses in attention maps, thereby prompting the semantics of the generated images.

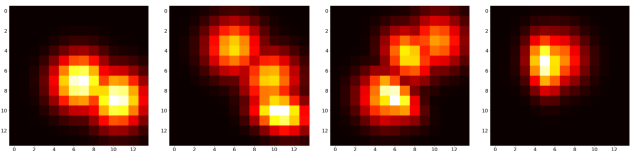


Figure 3. Examples of generated attention priors.

**Attention Priors Generation.** To generate attention priors  $\tilde{\mathbf{A}}_{l,h}$ , we employ GMM for it is the most commonly used distribution with high flexibility. ViTs utilize different attention heads to capture diverse patterns and learn varied, informative representations [8]. Thus, we use distinct GMMs for each head. Note that the goal here is not to replicate real attention maps precisely, but to generate simulated attention priors. These priors are used to explicitly encourage semantically meaningful regions within synthetic

images, prompting high responses in attention maps to enhance semantics.

In particular, we first initialize an all zero matrix  $\tilde{\mathbf{P}} \in \mathbb{R}^{H \times W}$ , where  $H = W = \sqrt{N-1}$  for DeiT,  $H = W = \sqrt{N}$  for Swin. For example, for DeiT-S, the  $H = W = \sqrt{196} = 14$ . Then, we generate  $k$  two-dimensional Gaussian distributions, where  $k$  is randomly sampled from  $1 \sim K_{APA}$  and  $K_{APA}$  is set to 5 in all experiments. Each Gaussian has its mean and covariance<sup>2</sup>. Consequently, the matrix element at the  $i$ -th row and  $j$ -th column,  $\tilde{\mathbf{P}}[i, j]$ , is determined by:

$$\tilde{\mathbf{P}}[i, j] = \max_{m=1, \dots, k} \mathbf{G}^m[i, j]. \quad (8)$$

Then,  $\tilde{\mathbf{P}}$  is normalized by:

$$\tilde{\mathbf{P}}_n = \frac{\tilde{\mathbf{P}}}{\sum \tilde{\mathbf{P}}} * (1 - x). \quad (9)$$

Here, for DeiT that incorporates the classification token,  $x$  is randomly sampled from a uniform distribution  $U(0, 1)$ , representing the proportion of the attention score that the classification token allocates to itself. For Swin, which does not use a classification token,  $x$  is set to 0. Finally,  $\tilde{\mathbf{P}}_n$  is flattened to match the dimensionality:

$$\tilde{\mathbf{A}}_{l,h} = \text{flatten}(\tilde{\mathbf{P}}_n). \quad (10)$$

Fig. 3 displays examples of generated attention priors. Although simple, APA effectively enhances semantics, as validated by both visualization and quantitative results. As shown in Fig. 1, compared to PSAQ-ViT, features after applying the APA loss are closer to the real images, indicating improved semantics. The quantitative results in Tab. 1 further support that APA achieves higher semantics. For instance, in Class 1, the intra-class similarity of PSAQ-ViT is 0.44, whereas APA achieves an improved similarity of 0.64.

### 3.3.2. Multi-Semantic Reinforcement

Current methods [43, 44, 58] optimize the entire synthetic image, restricting it to capture only the semantics of a single object type. However, this has two limitations. First, real images naturally exhibit low-rank properties, such as spatial similarity between nearby pixels [31]. Optimizing the entire images overlooks this structural regularity, easily leading to synthetic images with noisy or spurious regions that convey meaningless or misleading semantics [30]. This results in inefficient parameterization, where semantic contents available for model training are limited [34]. Second, real images often contain multiple objects with varied semantics. Constraining synthetic images to a single object type limits their semantic richness and diversity.

<sup>2</sup>The pseudo code is detailed in supplementary materials.

Motivated by the above analysis, we propose Multi-Semantic Reinforcement (MSR), which leverages localized patch optimization to promote efficient parameterization and diverse semantics. Specifically, for a synthetic image  $\tilde{\mathbf{I}}$ , instead of feeding only the entire image, we also feed its patches and optimize them individually. Initially, we select  $m$  non-overlapping patches, where  $m$  is chosen randomly from the set  $\{1, 2, \dots, K_{MSR}\}$ , with  $K_{MSR}$  set to 4 in all experiments. These  $m$  patches are then cropped and resized to match the model’s input dimensions:

$$\{\tilde{\mathbf{I}}_{MSR}^i\}_{i=1, \dots, m} = \text{resize}(\text{crop}_m(\tilde{\mathbf{I}})), \quad (11)$$

where  $\text{crop}_m(\cdot)$  crops  $m$  non-overlapping patches from input, and  $\text{resize}(\cdot)$  is the resize function. Each patch, denoted as  $\tilde{\mathbf{I}}_{MSR}^i$ , is treated as a new image with an assigned semantic target  $c^i$ . For simplicity, the loss function used to learn label-related semantics in both  $\tilde{\mathbf{I}}_{MSR}^i$  and  $\tilde{\mathbf{I}}$  is presented in Sec. 3.3.3. Note that the gradient is backpropagated only to update the corresponding patch in the original image, leaving the rest of the image unaffected.

By leveraging localized patch optimization, MSR effectively promotes efficient parameterization and diverse semantics in synthetic images. First, MSR reduces noisy and non-semantic regions and provides more distinct semantic samples, *i.e.*,  $\{\tilde{\mathbf{I}}_{MSR}^i\}_{i=1, \dots, m}$ , for model training, achieving efficient parameterization. Second, by assigning different semantic targets to individual cropped patches, MSR transforms synthetic images into composites of multiple semantic objects rather than a single uniform entity, thereby enhancing overall semantic diversity. Unlike traditional cropping used in data augmentation, which aims to improve classification robustness by training with cropped patches labeled with the original class, MSR aims to prompt efficient parameterization and semantic diversity within synthetic images, ultimately enabling accurate data-free quantization.

### 3.3.3. Softlabel Learning

The one-hot loss (Eq. 3) optimizes synthetic images until their confidence for the target class approaches 1. However, this leads to overfitting on a specific class, limiting semantic richness [77]. Moreover, Eq. 3 only learns the semantics of the target class, making it unsuitable for  $\tilde{\mathbf{I}}$  under MSR, as its patches  $\{\tilde{\mathbf{I}}_{MSR}^i\}_{i=1, \dots, m}$  contain distinct semantics.

To address this, we propose Softlabel Learning (SL), which softens the learning objective to promote more complex semantics and accommodate images augmented by MSR. Specifically, we first sample  $Z \in \mathbb{R}^C \sim U(0, 1)$ , then modify its values by:

$$\begin{cases} Z[c^i] \sim U(\epsilon_1, \epsilon_2), & \text{for } \tilde{\mathbf{I}}_{MSR}^i, \\ Z[c^1, \dots, c^m] \sim U(\epsilon_1, \epsilon_2), & \text{for } \tilde{\mathbf{I}}, \end{cases}$$

where  $U(\epsilon_1, \epsilon_2)$  denotes the uniform distribution over the interval  $[\epsilon_1, \epsilon_2]$ ,  $m$  is the number of patches determined in MSR, and  $\epsilon_1$  and  $\epsilon_2$  control the softness, both empirically set consistently to 5 and 10 in all experiments. The soft target is defined as  $T_s = \text{softmax}(Z)$ , and SL loss is:

$$\mathcal{L}^{\text{SL}}(\tilde{\mathbf{I}}/\tilde{\mathbf{I}}_{MSR}^i) = \text{SCE}(F(\tilde{\mathbf{I}}/\tilde{\mathbf{I}}_{MSR}^i), T_s), \quad (12)$$

where  $\text{SCE}(\cdot, \cdot)$  is soft cross entropy and  $F(\cdot)$  returns the predicted probability for its input.

For  $\tilde{\mathbf{I}}_{MSR}^i$ , SL aligns its predicted results with a ‘‘soft label’’ rather than a traditional one-hot label, mitigating overfitting and promoting the generation of semantically complex content. For  $\tilde{\mathbf{I}}$ , SL provides a suitable target for learning images with multiple semantic targets. Unlike the Soft Inception loss [77], which focuses only on the primary class probability, SL imposes a distribution across all classes, offering a comprehensive learning objective. Additionally, SL is compatible with MSR, where images contain multiple semantic targets. In contrast, the Soft Inception loss is designed for single-class scenarios and is therefore incompatible.

### 3.4. Overall Pipeline

The overall pipeline consists of two stages: data synthesis and quantized network learning. The first stage synthesizes synthetic images. The second stage fine-tunes the quantized model using the generated synthetic images.

#### 3.4.1. Data Synthesis

In the data synthesis stage, we combine the proposed APA loss of Eq. 7, SL loss of Eq. 12, and TV loss of Eq. 4 to formulate the objective function as follows:

$$\mathcal{L}_G(\tilde{\mathbf{I}}) = \alpha_1 \mathcal{L}^{\text{APA}}(\tilde{\mathbf{I}}) + \mathcal{L}^{\text{SL}}(\tilde{\mathbf{I}}) + 0.05 \mathcal{L}^{\text{TV}}(\tilde{\mathbf{I}}). \quad (13)$$

where  $\alpha_1$  is hyperparameters and is determined by grid-search. Note that the weight of TV loss is fixed to 0.05, following [43], to avoid a cumbersome hyperparameter search.

#### 3.4.2. Quantized Network Learning

Recently DFQ methods have introduced the PTQ methods in learning quantized models due to their advantages of speed, memory efficiency, and performance [32, 58]. Thus, following the success of [39, 64], we fine-tune the quantized network block-wisely. Specifically, denote  $\mathbf{X}_l$  as the outputs of the  $l$ -th block of the full-precision model, and  $\bar{\mathbf{X}}_l$  represent outputs of the quantized counterpart. The reconstruction loss is defined as:

$$\mathcal{L}_l = \|\mathbf{X}_l - \bar{\mathbf{X}}_l\|_2. \quad (14)$$

Here,  $\mathcal{L}_l$  is only backward to update weights within  $l$ -th block. Note that for a fair comparison, all compared methods adopt the same quantized network learning stage.

## 4. Experiment

### 4.1. Implementation Details

**Models and Datasets.** We evaluate the performance of the proposed SPDFQ across various ViTs on the image classification task, including ViT-S/B [19], DeiT-T/S/B [62], and Swin-S/B [50]. The dataset is ImageNet [59], which contains 1.28M training images and 50K validation images across 1,000 classes. The pre-trained models are downloaded from the timm library.

**Comparison methods.** We compare our SPDFQ against Gaussian noise, real images, and previous methods including SMI [30] and PSAQ-ViT [43] and its subsequent version, PSAQ-ViT V2 [44]. For a fair comparison, we generate synthetic images using their methods and apply our quantized network learning strategy. We use the official code for SMI and PSAQ-ViT to reproduce their images, while PSAQ-ViT V2 is re-implemented by us, as no official code is available.<sup>3</sup>

**Experimental settings.** All experiments use the PyTorch framework [56] on a single NVIDIA 3090 GPU. In the data synthesis stage, synthetic images were initialized with standard Gaussian noise, with 32 synthetic images generated in total. The Adam optimizer [35] with  $\beta_1 = 0.5$ ,  $\beta_2 = 0.9$  is employed. The learning rate is 0.25 for Swin and 0.2 for others, with a total of 1,000 iterations. For all models,  $K_{APA}$ ,  $K_{MSR}$ ,  $\epsilon_1$ , and  $\epsilon_2$  are respectively set to 5 and 4, 5, and 10, with these values are searched using W4A4 DeiT-S. The value of  $\alpha_1$  was determined by grid search for each model. Specifically,  $\alpha_1$  is set to  $1e5$  for DeiT-T/S,  $1e4$  for DeiT-B, 100 for ViT-B and Swin-B, 10 for Swin-S, and 1 for ViT-S. Although further searching hyperparameters may improve the performance, we use current settings since these already yield superior results. In the quantized network learning stage, the Adam optimizer with  $\beta_1 = 0.9$ ,  $\beta_2 = 0.999$  is employed. The weight decay is set to 0, and the initialized learning rate is  $4e-5$ , adjusted by the cosine decay strategy. The total iteration is set to 100. Consistent with [45], quantization parameters were determined by searching for percentile values that minimize quantization error before and after quantization. We follow the two-stage optimization strategy in [78] to optimize the quantized network. The channel-wise quantizer is adopted for weights and the layer-wise quantizer for activations. All matrix multiplications in ViTs are quantized [43–45].

### 4.2. Quantization Results

The quantization results are presented in Tab. 2. The proposed SPDFQ demonstrates consistent improvements across various quantization bit-width configurations, particularly with low bit-width settings. Specifically, for ViT-S,

<sup>3</sup>In supplementary materials, we present more comparisons with more methods on W8/A8 and W4/A8 settings.

Model	W/A	Real	Gaussian noise	PSAQ-ViT [43]	PSAQ-ViT V2 [44]	SMI [30]	SPDFQ (Ours)
ViT-S (81.39)	4/4	66.57	6.02	47.24	41.53	24.33 <sub>29.41</sub>	<b>50.32</b>
	5/5	76.69	36.77	71.59	68.41	61.33 <sub>65.19</sub>	<b>74.31</b>
	6/6	79.46	61.20	77.20	74.76	72.95 <sub>72.46</sub>	<b>78.40</b>
ViT-B (84.54)	4/4	68.16	0.15	36.32	26.32	35.27 <sub>19.67</sub>	<b>51.84</b>
	5/5	79.21	4.16	68.48	67.95	67.53 <sub>57.13</sub>	<b>70.70</b>
	6/6	81.89	55.18	76.65	71.87	76.33 <sub>69.82</sub>	<b>79.16</b>
DeiT-T (72.21)	4/4	56.60	17.43	47.75	30.20	30.14 <sub>13.18</sub>	<b>52.06</b>
	5/5	67.09	43.49	64.10	55.16	56.44 <sub>39.35</sub>	<b>66.41</b>
	6/6	69.81	56.23	68.37	62.77	64.03 <sub>44.39</sub>	<b>69.73</b>
DeiT-S (79.85)	4/4	68.46	20.89	58.28	45.53	42.77 <sub>11.71</sub>	<b>62.29</b>
	5/5	75.06	41.06	71.90	63.14	62.88 <sub>29.13</sub>	<b>74.06</b>
	6/6	77.87	65.63	75.85	68.85	71.65 <sub>37.69</sub>	<b>77.31</b>
DeiT-B (81.85)	4/4	77.07	47.20	71.75	66.43	65.33 <sub>59.04</sub>	<b>72.17</b>
	5/5	79.86	65.46	78.45	76.77	76.74 <sub>75.33</sub>	<b>78.72</b>
	6/6	80.90	62.79	80.00	79.22	78.81 <sub>77.66</sub>	<b>80.15</b>
Swin-S (83.20)	4/4	78.12	31.92	73.19	65.55	65.85	<b>74.74</b>
	5/5	80.51	52.10	78.15	74.37	75.41	<b>79.56</b>
	6/6	80.60	65.66	79.74	78.50	78.25	<b>80.56</b>
Swin-B (85.27)	4/4	78.80	30.14	71.84	67.42	65.23	<b>76.42</b>
	5/5	82.51	35.28	78.50	77.20	75.25	<b>80.82</b>
	6/6	82.64	67.37	82.00	81.41	80.30	<b>83.03</b>

Table 2. Quantization results on ImageNet dataset, with top-1 accuracy (%) reported. The performance of the full-precision model is listed below the model name. “W/A” denotes the bit-width of weights/activations. “Real” refers to using real images. For SMI [30], we provide the performance of using dense (normal-sized numbers) and sparse (smaller-sized numbers) synthetic images, respectively. Note that for Swin models, we do not provide the results for sparse synthetic images as the sparse generation method of SMI is infeasible.

SPDFQ improves the performance by 3.08% in the W4/A4 setting, 2.72% in the W5/A5 setting, and 1.20% in the W6/A6 setting. For ViT-B, SPDFQ achieves performance gains of 15.52% in the W4/A4 setting, 2.22% in the W5/A5 setting, and 2.51% in the W6/A6 setting. Results on DeiT also demonstrate the effectiveness of the proposed SPDFQ. For DeiT-T, SPDFQ shows a marked improvement by increasing top-1 accuracy by 4.31% in the W4/A4 setting, 2.31% in the W5/A5 setting, and 1.36% in the W6/A6 setting. For DeiT-S, SPDFQ enhances top-1 accuracy by 4.01% in the W4/A4 setting, 2.16% in the W5/A5 setting, and 1.46% in the W6/A6 setting. As for DeiT-B, SPDFQ enhances top-1 accuracy by 0.42% in the W4/A4 setting, 0.27% in the W5/A5 setting, and 0.15% in the W6/A6 setting. The quantization results of Swin-S/B also affirm the superiority of our SPDFQ in enhancing model accuracy under different quantization configurations. In particular, for Swin-S, the proposed SPDFQ increases the accuracy by 1.55% for the W4/A4 setting, 1.41% for the W5/A5 setting, and 0.82% for the W6/A6 setting, respectively. When it comes to Swin-B, the proposed SPDFQ increases the accuracy by 4.58% for the W4/A4 setting, 2.32% for the W5/A5

setting, and 1.03% for the W6/A6 setting, respectively.

### 4.3. Ablation Study

All ablation studies are conducted on the W4A4 DeiT-S.

APA	MSR	SL	Acc. (%)
Baseline			51.73
✓			60.26
	✓		50.75
		✓	52.02
✓	✓		61.58
✓		✓	60.51
	✓	✓	56.08
✓	✓	✓	<b>62.29</b>

Table 3. Influence of the proposed APA, MSR, and SL on accuracy. The baseline adopts the one-hot loss.

**Analysis of APA, MSR, and SL.** We first analyze the effectiveness of the proposed APA (Sec. 3.3.1), MSR (Sec. 3.3.2), and SL (Sec. 3.3.3). Experimental results are

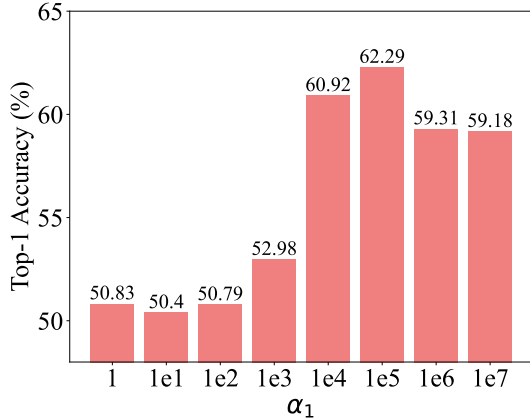


Figure 4. Ablation study of  $\alpha_1$ .

present in Tab. 3. It can be seen that when the APA and SL are individually added to synthesize fake images, the accuracy increases compared with the baseline. Notably, APA significantly boosts the baseline from 51.73% to 60.26%, supporting the analysis in Sec. 3.3.1 that demonstrates the APA’s effectiveness in enhancing semantics. In contrast, applying MSR alone slightly reduces accuracy from 51.73% to 50.75%, indicating that one-hot loss is unsuitable for synthetic images augmented with MSR. However, when both MSR and SL are applied, performance rises to 56.08%, suggesting that SL is more compatible with MSR than the one-hot loss. Combining APA with either MSR or SL further increases performance. For example, applying both APA and SL presents an accuracy of 60.51%. When all of the three strategies are applied, the best performance of 62.29% can be obtained.

**Analysis of priors distribution.** Tab. 4 showcases the results of using other distributions to formulate the attention priors. The unevenly distributed GMM and Laplace present comparable performance of 62.29% and 62.16%, respectively. Moreover, GMM provides a similar performance to the real’s, indicating it performs well in imitating the patterns of real images.

**Analysis of  $\alpha_1$ ,  $K_{APA}$ , and  $K_{MSR}$ .** The  $\alpha_1$  from Eq. 13 balance the importance of the proposed APA loss during the update of the synthetic images. Fig. 4 demonstrates that the optimal performance is achieved when  $\alpha_1 = 1e5$ . Incrementally increasing  $\alpha_1$  improves performance up to 62.29% at  $\alpha_1 = 1e5$ . However, further increases in  $\alpha_1$  subsequently degrade performance.

The  $K_{APA}$  in APA is the upper limit on the number of the Gaussian distributions used for priors generation. Tab. 5 displays the ablation study for different values of  $K_{APA}$ . The best accuracy is achieved when  $K_{APA} = 5$ .

The  $K_{MSR}$  in MSR is the upper limit on the number of patches. Fig. 5 demonstrates that when  $K_{MSR} = 4$ , the optimal performance is achieved. Using  $K_{MSR}$  larger than

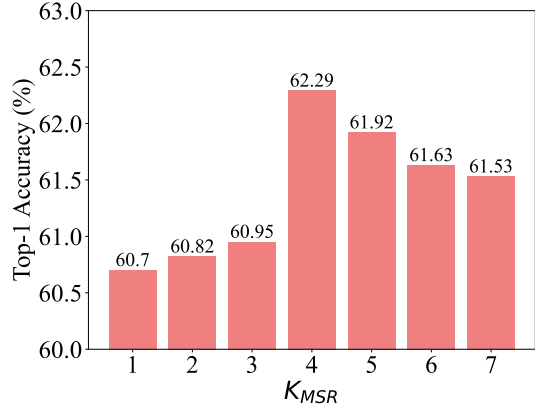


Figure 5. Ablation study of  $K_{MSR}$ .

Priors Distribution	Top-1	$K_{APA}$	Top-1
GMM	62.29	1	61.13
Laplace	62.16	3	61.52
Real	<b>63.19</b>	5	<b>62.29</b>
		7	61.53
		9	61.05

Table 4. Effect of priors type.

Table 5. Effect of  $K_{APA}$ .

S	Top-1
0	61.96
$L/2$	<b>62.29</b>

Table 6. Effect of  $S$ .

w. $\frac{1}{L}$	Top-1
✓	<b>62.29</b>
×	61.32

Table 7. Effect of  $\frac{1}{L}$ .

4 will hurt the accuracy. We consider this due to limited patch resolution if using a too large  $K_{MSR}$ .

**Analysis of APA loss.** Here, we conduct the ablation study by considering the  $S$  and scale  $\frac{1}{L}$  in Eq. 7. Tab. 6 presents the effect of varying  $S$  in Eq. 7. If applying APA loss to all blocks ( $S = 0$ ), the top-1 accuracy decreases to 61.96%. From Tab. 7, it can be seen that absorbing the scale  $\frac{1}{L}$  in Eq. 7 presents 0.97% performance gains.

## 5. Limitations

We further discuss some limitations of the proposed SPDFQ, which will guide future research directions. First, although SPDFQ shows substantial performance improvement, a performance gap between SPDFQ and real data remains challenging. Further enhancing semantic alignment between synthetic and real images could help close this gap, highlighting the need for a more precise semantics prompting method. Second, SPDFQ currently lacks a theoretical foundation. Theoretical exploration would be beneficial for gaining more insight into the DFQ for ViTs.



## 6. Conclusion

In this paper, we investigate DFQ specifically designed for ViTs. We first identify that synthetic images generated by existing methods suffer from the deficient semantics issue, where the semantics deviate from the real images, leading to limited performance. To address this, we propose a novel DFQ method, dubbed SPDFQ, which introduces three key innovations: Attention Priors Alignment (APA), Multi-Semantic Reinforcement (MSR), and Softlabel Learning (SL). APA encourages high responses in attention maps to prompt semantics in synthetic images. MSR promotes efficient parameterization and semantic diversity. SL enables the generation of complex semantics in synthetic images and accommodates images augmented by MSR. Extensive experiments across various ViT models demonstrate the effectiveness of SPDFQ.

## References

- [1] Anurag Arnab, Mostafa Dehghani, Georg Heigold, Chen Sun, Mario Lučić, and Cordelia Schmid. Vivit: A video vision transformer. In *Proceedings of the IEEE/CVF international conference on computer vision (ICCV)*, pages 6836–6846, 2021. 1, 2
- [2] Jianhong Bai, Yuchen Yang, Huanpeng Chu, Hualiang Wang, Zuozhu Liu, Ruizhe Chen, Xiaoxuan He, Lianrui Mu, Chengfei Cai, and Haoji Hu. Robustness-guided image synthesis for data-free quantization. *arXiv preprint arXiv:2310.03661*, 2023. 2
- [3] Ron Banner, Yury Nahshan, Daniel Soudry, et al. Post training 4-bit quantization of convolutional networks for rapid-deployment. In *Proceedings of the Advances in Neural Information Processing Systems (NeurIPS)*, pages 7950–7958, 2019. 2
- [4] Yoshua Bengio, Aaron Courville, and Pascal Vincent. Representation learning: A review and new perspectives. *IEEE Transactions on Pattern Analysis and Machine Intelligence (TPAMI)*, 35(8):1798–1828, 2013. 3
- [5] Daniel Bolya, Cheng-Yang Fu, Xiaoliang Dai, Peizhao Zhang, Christoph Feichtenhofer, and Judy Hoffman. Token merging: Your vit but faster. In *The Eleventh International Conference on Learning Representations (ICLR)*, 2023. 4
- [6] Yaohui Cai, Zhewei Yao, Zhen Dong, Amir Gholami, Michael W Mahoney, and Kurt Keutzer. Zeroq: A novel zero shot quantization framework. In *Proceedings of the IEEE/CVF Conference on Computer Vision and Pattern Recognition (CVPR)*, pages 13169–13178, 2020. 1, 2
- [7] Nicolas Carion, Francisco Massa, Gabriel Synnaeve, Nicolas Usunier, Alexander Kirillov, and Sergey Zagoruyko. End-to-end object detection with transformers. In *Proceedings of the European Conference on Computer Vision (ECCV)*, pages 213–229. Springer, 2020. 1, 2
- [8] Hila Chefer, Shir Gur, and Lior Wolf. Generic attention-model explainability for interpreting bi-modal and encoder-decoder transformers. In *Proceedings of the IEEE/CVF International Conference on Computer Vision (ICCV)*, pages 397–406, 2021. 4
- [9] Hanqing Chen, Yunhe Wang, Tianyu Guo, Chang Xu, Yiping Deng, Zhenhua Liu, Siwei Ma, Chunjing Xu, Chao Xu, and Wen Gao. Pre-trained image processing transformer. In *Proceedings of the IEEE/CVF Conference on Computer Vision and Pattern Recognition (CVPR)*, pages 12299–12310, 2021. 2
- [10] Mengzhao Chen, Mingbao Lin, Ke Li, Yunhang Shen, Yongjian Wu, Fei Chao, and Rongrong Ji. Cf-vit: A general coarse-to-fine method for vision transformer. In *Proceedings of the AAAI Conference on Artificial Intelligence*, pages 7042–7052, 2023. 4
- [11] Mengzhao Chen, Wenqi Shao, Peng Xu, Mingbao Lin, Kaipeng Zhang, Fei Chao, Rongrong Ji, Yu Qiao, and Ping Luo. Difftrate: Differentiable compression rate for efficient vision transformers. In *Proceedings of the IEEE/CVF Conference on Computer Vision and Pattern Recognition (CVPR)*, pages 17164–17174, 2023. 1
- [12] Xin Chen, Bin Yan, Jiawen Zhu, Dong Wang, Xiaoyun Yang, and Huchuan Lu. Transformer tracking. In *Proceedings of the IEEE/CVF Conference on Computer Vision and Pattern Recognition (CVPR)*, pages 8126–8135, 2021. 2
- [13] Xinrui Chen, Yizhi Wang, Renao Yan, Yiqing Liu, Tian Guan, and Yonghong He. Texq: Zero-shot network quantization with texture feature distribution calibration. In *Proceedings of the Advances in Neural Information Processing Systems (NeurIPS)*, 2024. 2
- [14] Kanghyun Choi, Deokki Hong, Noseong Park, Youngsok Kim, and Jinho Lee. Qimera: Data-free quantization with synthetic boundary supporting samples. In *Proceedings of the Advances in Neural Information Processing Systems (NeurIPS)*, pages 14835–14847, 2021. 1
- [15] Kanghyun Choi, Hye Yoon Lee, Deokki Hong, Joonsang Yu, Noseong Park, Youngsok Kim, and Jinho Lee. It’s all in the teacher: Zero-shot quantization brought closer to the teacher. In *Proceedings of the IEEE/CVF Conference on Computer Vision and Pattern Recognition (CVPR)*, pages 8311–8321, 2022. 2
- [16] Kanghyun Choi, Hye Yoon Lee, Dain Kwon, SunJong Park, Kyuyeun Kim, Noseong Park, and Jinho Lee. MimiQ: Low-bit data-free quantization of vision transformers. *arXiv preprint arXiv:2407.20021*, 2024. 2, 3
- [17] Jean-Baptiste Cordonnier, Andreas Loukas, and Martin Jaggi. On the relationship between self-attention and convolutional layers. In *Proceedings of the International Conference on Learning Representations (ICLR)*, 2020. 4
- [18] Yifu Ding, Haotong Qin, Qinghua Yan, Zhenhua Chai, Junjie Liu, Xiaolin Wei, and Xianglong Liu. Towards accurate post-training quantization for vision transformer. In *Proceedings of the 30th ACM International Conference on Multimedia (ACMMM)*, pages 5380–5388, 2022. 2
- [19] Alexey Dosovitskiy, Lucas Beyer, Alexander Kolesnikov, Dirk Weissenborn, Xiaohua Zhai, Thomas Unterthiner, Mostafa Dehghani, Matthias Minderer, Georg Heigold, Sylvain Gelly, et al. An image is worth 16x16 words: Transformers for image recognition at scale. In *Proceedings of*

- the International Conference on Learning Representations (ICLR)*, 2021. 1, 2, 4, 6
- [20] Steven K. Esser, Jeffrey L. McKinstry, Deepika Bablani, Rathinakumar Appuswamy, and Dharmendra S. Modha. Learned step size quantization. In *Proceedings of the International Conference on Learning Representations (ICLR)*, 2020. 2
- [21] Natalia Frumkin, Dibakar Gope, and Diana Marculescu. Jumping through local minima: Quantization in the loss landscape of vision transformers. In *Proceedings of the IEEE/CVF International Conference on Computer Vision (ICCV)*, pages 16978–16988, 2023. 2, 3
- [22] Ruihao Gong, Xianglong Liu, Shenghu Jiang, Tianxiang Li, Peng Hu, Jiazhen Lin, Fengwei Yu, and Junjie Yan. Differentiable soft quantization: Bridging full-precision and low-bit neural networks. In *Proceedings of the IEEE/CVF Conference on Computer Vision and Pattern Recognition (CVPR)*, pages 4852–4861, 2019. 2
- [23] Ian J. Goodfellow, Jean Pouget-Abadie, Mehdi Mirza, Bing Xu, David Warde-Farley, Sherjil Ozair, Aaron Courville, and Yoshua Bengio. Generative adversarial nets. In *Proceedings of the Advances in Neural Information Processing Systems (NeurIPS)*, pages 2672–2680, 2014. 3
- [24] Cong Guo, Yuxian Qiu, Jingwen Leng, Xiaotian Gao, Chen Zhang, Yunxin Liu, Fan Yang, Yuhao Zhu, and Minyi Guo. Squant: On-the-fly data-free quantization via diagonal hessian approximation. In *The Eleventh International Conference on Learning Representations (ICLR)*, 2022. 1, 2
- [25] Kai Han, An Xiao, Enhua Wu, Jianyuan Guo, Chunjing Xu, and Yunhe Wang. Transformer in transformer. In *Proceedings of the Advances in Neural Information Processing Systems (NeurIPS)*, 2021. 2
- [26] Kai Han, Yunhe Wang, Hanting Chen, Xinghao Chen, Jianyuan Guo, Zhenhua Liu, Yehui Tang, An Xiao, Chunjing Xu, Yixing Xu, et al. A survey on vision transformer. *IEEE Transactions on Pattern Analysis and Machine Intelligence (TPAMI)*, 45(1):87–110, 2022. 1
- [27] Zhiwei Hao, Jianyuan Guo, Ding Jia, Kai Han, Yehui Tang, Chao Zhang, Han Hu, and Yunhe Wang. Learning efficient vision transformers via fine-grained manifold distillation. In *Proceedings of the Advances in Neural Information Processing Systems (NeurIPS)*, 2021. 1
- [28] Joakim Bruslund Haurum, Sergio Escalera, Graham W Taylor, and Thomas B Moeslund. Which tokens to use? investigating token reduction in vision transformers. In *Proceedings of the IEEE/CVF Conference on Computer Vision and Pattern Recognition (CVPR)*, pages 773–783, 2023. 4
- [29] Zejiang Hou and Sun-Yuan Kung. Multi-dimensional vision transformer compression via dependency guided gaussian process search. In *Proceedings of the IEEE/CVF Conference on Computer Vision and Pattern Recognition (CVPR)*, pages 3669–3678, 2022. 1
- [30] Zixuan Hu, Yongxian Wei, Li Shen, Zhenyi Wang, Lei Li, Chun Yuan, and Dacheng Tao. Sparse model inversion: Efficient inversion of vision transformers for data-free applications. In *Proceedings of the International Conference on Machine Learning (ICML)*. 2, 3, 5, 6, 7
- [31] Jingtang Huang and David Mumford. Statistics of natural images and models. In *Proceedings. 1999 IEEE Computer Society Conference on Computer Vision and Pattern Recognition*, pages 541–547. IEEE, 1999. 5
- [32] Yongkweon Jeon, Chungman Lee, and Ho-young Kim. Genie: show me the data for quantization. In *Proceedings of the IEEE/CVF Conference on Computer Vision and Pattern Recognition (CVPR)*, pages 12064–12073, 2023. 2, 6
- [33] Salman Khan, Muzammal Naseer, Munawar Hayat, Syed Waqas Zamir, Fahad Shahbaz Khan, and Mubarak Shah. Transformers in vision: A survey. *ACM Computing Surveys (CSUR)*, 2021. 1
- [34] Jang-Hyun Kim, Jinuk Kim, Seong Joon Oh, Sangdoon Yun, Hwanjun Song, Joonhyun Jeong, Jung-Woo Ha, and Hyun Oh Song. Dataset condensation via efficient synthetic-data parameterization. In *Proceedings of the International Conference on Machine Learning (ICML)*, pages 11102–11118. PMLR, 2022. 5
- [35] Diederik P Kingma and Jimmy Ba. Adam: A method for stochastic optimization. In *Proceedings of the International Conference on Learning Representations (ICLR)*, 2014. 6
- [36] Raghuraman Krishnamoorthi. Quantizing deep convolutional networks for efficient inference: A whitepaper. *arXiv preprint arXiv:1806.08342*, 2018. 1
- [37] Huantong Li, Xiangmiao Wu, Fanbing Lv, Daihai Liao, Thomas H Li, Yonggang Zhang, Bo Han, and Minghui Tan. Hard sample matters a lot in zero-shot quantization. In *Proceedings of the IEEE/CVF Conference on Computer Vision and Pattern Recognition (CVPR)*, pages 24417–24426, 2023. 2
- [38] Yuhang Li, Xin Dong, and Wei Wang. Additive powers-of-two quantization: An efficient non-uniform discretization for neural networks. In *Proceedings of the International Conference on Learning Representations (ICLR)*, 2020. 2
- [39] Yuhang Li, Ruihao Gong, Xu Tan, Yang Yang, Peng Hu, Qi Zhang, Fengwei Yu, Wei Wang, and Shi Gu. Brecq: Pushing the limit of post-training quantization by block reconstruction. In *Proceedings of the International Conference on Learning Representations (ICLR)*, 2021. 2, 6
- [40] Yanjing Li, Sheng Xu, Baochang Zhang, Xianbin Cao, Peng Gao, and Guodong Guo. Q-vit: Accurate and fully quantized low-bit vision transformer. In *Proceedings of the Advances in Neural Information Processing Systems (NeurIPS)*, pages 34451–34463, 2022. 2
- [41] Yuhang Li, Youngeun Kim, Donghyun Lee, and Priyadarshini Panda. Stableq: Enhancing data-scarce quantization with text-to-image data. *arXiv preprint arXiv:2312.05272*, 2023. 2
- [42] Zhikai Li and Qingyi Gu. I-vit: Integer-only quantization for efficient vision transformer inference. In *Proceedings of the IEEE/CVF International Conference on Computer Vision (ICCV)*, pages 17065–17075, 2023. 1, 2
- [43] Zhikai Li, Liping Ma, Mengjuan Chen, Junrui Xiao, and Qingyi Gu. Patch similarity aware data-free quantization for vision transformers. In *Proceedings of the European Conference on Computer Vision (ECCV)*, pages 154–170. Springer, 2022. 1, 2, 3, 4, 5, 6, 7

- [44] Zhikai Li, Mengjuan Chen, Junrui Xiao, and Qingyi Gu. Psaq-vit v2: Toward accurate and general data-free quantization for vision transformers. *IEEE Transactions on Neural Networks and Learning Systems (TNNLS)*, 2023. 2, 3, 5, 6, 7
- [45] Zhikai Li, Junrui Xiao, Lianwei Yang, and Qingyi Gu. Repq-vit: Scale reparameterization for post-training quantization of vision transformers. In *Proceedings of the IEEE/CVF International Conference on Computer Vision (ICCV)*, pages 17227–17236, 2023. 3, 6
- [46] Jingyun Liang, Jiezhong Cao, Guolei Sun, Kai Zhang, Luc Van Gool, and Radu Timofte. Swinir: Image restoration using swin transformer. In *Proceedings of the IEEE/CVF international conference on computer vision (ICCV)*, pages 1833–1844, 2021. 2
- [47] Yang Lin, Tianyu Zhang, Peiqin Sun, Zheng Li, and Shuchang Zhou. Fq-vit: Post-training quantization for fully quantized vision transformer. In *Proceedings of the Thirty-First International Joint Conference on Artificial Intelligence, (IJCAI)*, pages 1173–1179, 2022. 2, 3
- [48] Shih-Yang Liu, Zechun Liu, and Kwang-Ting Cheng. Oscillation-free quantization for low-bit vision transformers. In *Proceedings of the International Conference on Machine Learning (ICML)*, pages 21813–21824, 2023. 2
- [49] Yijiang Liu, Huanrui Yang, Zhen Dong, Kurt Keutzer, Li Du, and Shanghang Zhang. Noisyquant: Noisy bias-enhanced post-training activation quantization for vision transformers. In *Proceedings of the IEEE/CVF Conference on Computer Vision and Pattern Recognition (CVPR)*, pages 20321–20330, 2023. 2
- [50] Ze Liu, Yutong Lin, Yue Cao, Han Hu, Yixuan Wei, Zheng Zhang, Stephen Lin, and Baining Guo. Swin transformer: Hierarchical vision transformer using shifted windows. In *Proceedings of the IEEE/CVF international conference on computer vision (ICCV)*, pages 10012–10022, 2021. 2, 6
- [51] Zhenhua Liu, Yunhe Wang, Kai Han, Wei Zhang, Siwei Ma, and Wen Gao. Post-training quantization for vision transformer. In *Proceedings of the Advances in Neural Information Processing Systems (NeurIPS)*, pages 28092–28103, 2021. 1, 2
- [52] Yiwei Ma, Jiayi Ji, Xiaoshuai Sun, Yiyi Zhou, and Rongrong Ji. Towards local visual modeling for image captioning. *Pattern Recognition*, 138:109420, 2023. 1
- [53] Sachin Mehta and Mohammad Rastegari. Mobilevit: Lightweight, general-purpose, and mobile-friendly vision transformer. In *Proceedings of the International Conference on Learning Representations (ICLR)*, 2022. 2
- [54] Muhammad Muzammal Naseer, Kanchana Ranasinghe, Salman H Khan, Munawar Hayat, Fahad Shahbaz Khan, and Ming-Hsuan Yang. Intriguing properties of vision transformers. In *Proceedings of the Advances in Neural Information Processing Systems (NeurIPS)*, pages 23296–23308, 2021. 3
- [55] Daniel Neimark, Omri Bar, Maya Zohar, and Dotan Asselmann. Video transformer network. In *Proceedings of the IEEE/CVF International Conference on Computer Vision (ICCV)*, pages 3163–3172, 2021. 2
- [56] Adam Paszke, Sam Gross, Francisco Massa, Adam Lerer, James Bradbury, Gregory Chanan, Trevor Killeen, Zeming Lin, Natalia Gimelshein, Luca Antiga, et al. Pytorch: An imperative style, high-performance deep learning library. In *Proceedings of the Advances in Neural Information Processing Systems (NeurIPS)*, pages 8026–8037, 2019. 6
- [57] Biao Qian, Yang Wang, Richang Hong, and Meng Wang. Adaptive data-free quantization. In *Proceedings of the IEEE/CVF Conference on Computer Vision and Pattern Recognition (CVPR)*, pages 7960–7968, 2023. 2
- [58] Akshat Ramchandran, Souvik Kundu, and Tushar Krishna. Clamp-vit: contrastive data-free learning for adaptive post-training quantization of vits. In *Proceedings of the European Conference on Computer Vision (ECCV)*. Springer, 2024. 2, 3, 5, 6
- [59] Olga Russakovsky, Jia Deng, Hao Su, Jonathan Krause, Sanjeev Satheesh, Sean Ma, Zhiheng Huang, Andrej Karpathy, Aditya Khosla, Michael Bernstein, et al. Imagenet large scale visual recognition challenge. *International Journal of Computer Vision (IJCV)*, 115:211–252, 2015. 6
- [60] Fahad Shamshad, Salman Khan, Syed Waqas Zamir, Muhammad Haris Khan, Munawar Hayat, Fahad Shahbaz Khan, and Huazhu Fu. Transformers in medical imaging: A survey. *Medical Image Analysis*, page 102802, 2023. 2
- [61] Yehui Tang, Kai Han, Yunhe Wang, Chang Xu, Jianyuan Guo, Chao Xu, and Dacheng Tao. Patch slimming for efficient vision transformers. In *Proceedings of the IEEE/CVF Conference on Computer Vision and Pattern Recognition (CVPR)*, pages 12165–12174, 2022. 1
- [62] Hugo Touvron, Matthieu Cord, Matthijs Douze, Francisco Massa, Alexandre Sablayrolles, and Hervé Jégou. Training data-efficient image transformers & distillation through attention. In *Proceedings of the International Conference on Machine Learning (ICML)*, pages 10347–10357. PMLR, 2021. 1, 2, 6
- [63] Laurens van der Maaten and Geoffrey Hinton. Visualizing data using t-sne. *Journal of Machine Learning Research (JMLR)*, 9:2579–2605, 2008. 1, 2, 3
- [64] Xiuying Wei, Ruihao Gong, Yuhang Li, Xianglong Liu, and Fengwei Yu. Qdrop: Randomly dropping quantization for extremely low-bit post-training quantization. In *Proceedings of the International Conference on Learning Representations (ICLR)*, 2022. 6
- [65] Kan Wu, Houwen Peng, Minghao Chen, Jianlong Fu, and Hongyang Chao. Rethinking and improving relative position encoding for vision transformer. In *Proceedings of the IEEE/CVF International Conference on Computer Vision (ICCV)*, pages 10033–10041, 2021. 2
- [66] Kan Wu, Jinnian Zhang, Houwen Peng, Mengchen Liu, Bin Xiao, Jianlong Fu, and Lu Yuan. Tinyvit: Fast pretraining distillation for small vision transformers. In *Proceedings of the European Conference on Computer Vision (ECCV)*, pages 68–85, 2022. 2
- [67] Zhiqiang Shen Xijie Huang and Kwang-Ting Cheng. Variation-aware vision transformer quantization. *arXiv preprint arXiv:2307.00331*, 2023. 2
- [68] Shoukai Xu, Haokun Li, Bohan Zhuang, Jing Liu, Jiezhong Cao, Chuangrun Liang, and Mingkui Tan. Generative low-bitwidth data free quantization. In *Proceedings of the Euro-*

- pean Conference on Computer Vision (ECCV), pages 1–17, 2020. [3](#)
- [69] Shoukai Xu, Haokun Li, Bohan Zhuang, Jing Liu, Jiezhong Cao, Chuangrun Liang, and Mingkui Tan. Generative low-bitwidth data free quantization. In *Proceedings of the European Conference on Computer Vision (ECCV)*, pages 1–17. Springer, 2020. [1](#), [2](#)
- [70] Hongxu Yin, Pavlo Molchanov, Jose M Alvarez, Zhizhong Li, Arun Mallya, Derek Hoiem, Niraj K Jha, and Jan Kautz. Dreaming to distill: Data-free knowledge transfer via deep-inversion. In *Proceedings of the IEEE/CVF Conference on Computer Vision and Pattern Recognition (CVPR)*, pages 8715–8724, 2020. [1](#), [3](#)
- [71] Jason Yosinski, Jeff Clune, Anh Nguyen, Thomas Fuchs, and Hod Lipson. Understanding neural networks through deep visualization. *arXiv preprint arXiv:1506.06579*, 2015. [3](#)
- [72] Matthew D. Zeiler and Rob Fergus. Visualizing and understanding convolutional networks. In *Proceedings of the IEEE/CVF International Conference on Computer Vision (ICCV)*, pages 818–833, 2014. [3](#)
- [73] Jinnian Zhang, Houwen Peng, Kan Wu, Mengchen Liu, Bin Xiao, Jianlong Fu, and Lu Yuan. Minivit: Compressing vision transformers with weight multiplexing. In *Proceedings of the IEEE/CVF Conference on Computer Vision and Pattern Recognition (CVPR)*, pages 12145–12154, 2022. [2](#)
- [74] Xiangguo Zhang, Haotong Qin, Yifu Ding, Ruihao Gong, Qinghua Yan, Renshuai Tao, Yuhang Li, Fengwei Yu, and Xianglong Liu. Diversifying sample generation for accurate data-free quantization. In *Proceedings of the IEEE/CVF Conference on Computer Vision and Pattern Recognition (CVPR)*, pages 15658–15667, 2021. [1](#), [2](#)
- [75] Dehua Zheng, Wenhui Dong, Hailin Hu, Xinghao Chen, and Yunhe Wang. Less is more: Focus attention for efficient detr. In *Proceedings of the IEEE/CVF International Conference on Computer Vision (ICCV)*, pages 6674–6683, 2023. [1](#)
- [76] Sixiao Zheng, Jiachen Lu, Hengshuang Zhao, Xiatian Zhu, Zekun Luo, Yabiao Wang, Yanwei Fu, Jianfeng Feng, Tao Xiang, Philip HS Torr, et al. Rethinking semantic segmentation from a sequence-to-sequence perspective with transformers. In *Proceedings of the IEEE/CVF conference on computer vision and pattern recognition (CVPR)*, pages 6881–6890, 2021. [2](#)
- [77] Yunshan Zhong, Mingbao Lin, Gongrui Nan, Jianzhuang Liu, Baochang Zhang, Yonghong Tian, and Rongrong Ji. Intraq: Learning synthetic images with intra-class heterogeneity for zero-shot network quantization. In *Proceedings of the IEEE/CVF Conference on Computer Vision and Pattern Recognition (CVPR)*, pages 12339–12348, 2022. [1](#), [2](#), [5](#), [6](#)
- [78] Yunshan Zhong, Jiawei Hu, Mingbao Lin, Mengzhao Chen, and Rongrong Ji. I&s-vit: An inclusive & stable method for pushing the limit of post-training vits quantization. *arXiv preprint arXiv:2311.10126*, 2023. [6](#)
- [79] Yunshan Zhong, Jiawei Hu, You Huang, Yuxin Zhang, and Rongrong Ji. Erq: Error reduction for post-training quantization of vision transformers. In *Proceedings of the International Conference on Machine Learning (ICML)*, 2024. [2](#)

# Semantics Prompting Data-Free Quantization for Low-Bit Vision Transformers

## Supplementary Material

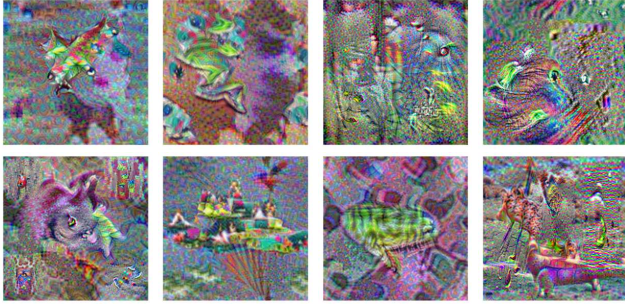


Figure 1. The fake samples (224×224) generated using SPDFQ.

```

1
2 from scipy.stats import multivariate_normal
3 import numpy as np
4
5 def Single_Gaussian():
6     mean = np.random.uniform(-5, 5, 2)
7     covariance = None
8     while True:
9         A = np.random.uniform(0, 1, (2, 2)) * 10
10        covariance = np.dot(A, A.T)
11        try:
12            eigenvalues, eigenvectors = np.linalg.eig(covariance)
13            eigenvalues = np.clip(eigenvalues, 0, 5)
14            covariance = np.dot(np.dot(eigenvectors,
15                                     np.diag(eigenvalues)), eigenvectors.T)
16            return multivariate_normal(mean, covariance)
17        except np.linalg.LinAlgError:
18            continue

```

### 1. Code to Gaussian Distribution Generation

In the following code, we provide the Python code for generating the Gaussian used in our paper.

### 2. Examples of Generated Images.

Fig. 1 shows the visualization results of the generated images (224×224) using the proposed SPDFQ. It can be seen that generated images possess foreground, despite the foreground being rough. Also, it is worth noting that the generated image typically possesses hard-to-identify unreal texture [? ]. The sensory quality of generated data is not relevant to downstream tasks. As shown in [? ? ? ], recent zero-shot quantization methods (TexQ [? ], Qimera [? ], Intraq [? ], and so on) produce images with low sensory quality. However, these methods still achieve significant performance improvements. As a result, the effectiveness of generated images for downstream tasks cannot be judged solely by their sensory quality. We encourage the reader to focus more on the semantics distribution extracted by the model as shown in Fig. 1 in the main paper.

$\epsilon_1$	Top-1
1	61.00
3	61.05
5	<b>62.29</b>
7	61.15
9	61.36

Table 1. Effect of  $\epsilon_1$ .

$\epsilon_2$	Top-1
6	61.62
8	61.88
10	<b>62.29</b>
12	62.13
14	61.10

Table 2. Effect of  $\epsilon_2$ .

### 3. More Ablation Study

The  $\epsilon_1$  and  $\epsilon_2$  in SL balance the smoothness of the proposed SL loss. Tab. 1 demonstrates that the optimal performance is achieved when  $\epsilon_1 = 5$ . Incrementally increasing  $\epsilon_1$  from 1 to 5 improves performance from 61.00% to 62.29%. Then, further increasing  $\epsilon_1$  subsequently degrades performance. For example, increasing  $\epsilon_1$  to 9 results in 0.93% degradation. Tab. 2 presents the ablation study of  $\epsilon_2$ . It can be seen that the optimal performance is achieved when  $\epsilon_2 = 10$ . Using smaller or larger values than 10 will hurt the performance.

### 4. Additional Quantization Results

#### 4.1. Classification Results

Tab. 3 presents the quantization results for the W8A8 and W4A8 settings. Here, we use a linear quantizer for attention scores, which is consistent with the compared methods. The results of the compared methods are copied from their paper. It can be observed that the proposed SPDFQ outperforms the compared methods in most cases, except for W8A8 DeiT-T, where SPDFQ exhibits only a 0.05% gap. Notably, SPDFQ generally provides larger performance gains in the W4A8 setting. For instance, SPDFQ achieves increases of 1.24% and 0.70% on W4A8 DeiT-S and DeiT-B, respectively. These results clearly demonstrate the effectiveness of the proposed SPDFQ.

#### 4.2. Detection and Segmentation Results

In Tab. 4, we provide the results on detection and segmentation tasks. Note that results with “†” are re-produced by ours and the other results of PSAQ-ViT V2 [? ] and CLAMP-ViT [? ] are copied from their paper. Following [? ? ], the results are evaluated on Mask R-CNN and Cascade R-CNN models, both with Swin-S as the backbone. The proposed SPDFQ consistently outperforms the compared methods. For example, SPDFQ achieves 1.2 and 2.9 increases on box and mask AP for W4A8 Mask R-CNN,

Model	W/A	PSAQ-ViT [? ]	PSAQ-ViT V2 [? ]	SMI [? ]	CLAMP-ViT [? ]	SPDFQ (Ours)
ViT-S (81.39)	8/8	31.45	-	-	-	<b>80.81</b>
	4/8	20.84	-	-	-	<b>78.49</b>
ViT-B (84.54)	8/8	37.36	-	-	84.19	<b>84.22</b>
	4/8	25.34	-	-	78.73	<b>82.19</b>
DeiT-T (72.21)	8/8	71.56	72.17	70.27 <sub>70.13</sub>	72.17	72.12
	4/8	65.57	68.61	64.28 <sub>64.04</sub>	69.93	<b>70.05</b>
DeiT-S (79.85)	8/8	76.92	79.56	-	79.55	<b>79.81</b>
	4/8	73.23	76.36	-	77.03	<b>78.27</b>
DeiT-B (81.85)	8/8	79.10	81.52	75.99 <sub>77.51</sub>	-	<b>81.83</b>
	4/8	77.05	79.49	78.58 <sub>79.63</sub>	-	<b>80.19</b>
Swin-T (81.35)	8/8	75.35	80.21	-	81.17	<b>81.18</b>
	4/8	71.79	76.28	-	80.28	<b>80.34</b>
Swin-S (83.20)	8/8	76.64	82.13	-	82.57	<b>82.85</b>
	4/8	75.14	78.86	-	<b>82.51</b>	<b>82.51</b>

Table 3. Quantization results on ImageNet dataset, with top-1 accuracy (%) reported. The performance of the full-precision model is listed below the model name, “W/A” denotes the bit-width of weights/activations. The results of PSAQ-ViT [? ], PSAQ-ViT V2 [? ], SMI [? ], and CLAMP-ViT [? ] are copied from their paper, and “-” denotes the results are unavailable. For SMI [? ], we provide the performance of using dense (normal-sized numbers) and sparse (smaller-sized numbers) synthetic images, respectively.

Model	W/A	Method	AP (box)	AP (mask)
Mask R-CNN (Swin-S)	32/32	-	48.5	43.3
	4/8	PSAQ-ViT V2 <sup>†</sup> [? ]	44.7	39.0
		SPDFQ (Ours)	<b>45.9</b>	<b>41.9</b>
	8/8	PSAQ-ViT V2 <sup>†</sup> [? ]	47.8	42.7
SPDFQ (Ours)		<b>48.2</b>	<b>43.0</b>	
Cascade R-CNN (Swin-S)	32/32	-	51.8	44.7
	4/8	PSAQ-ViT V2 [? ]	47.9	41.4
		PSAQ-ViT V2 <sup>†</sup> [? ]	48.2	42.7
		CLAMP-ViT [? ]	48.5	42.2
		SPDFQ (Ours)	<b>49.0</b>	<b>42.9</b>
	8/8	PSAQ-ViT V2 [? ]	50.9	44.1
		PSAQ-ViT V2 <sup>†</sup> [? ]	51.0	44.2
		CLAMP-ViT [? ]	51.4	<b>44.6</b>
SPDFQ (Ours)		<b>51.7</b>	<b>44.6</b>	

Table 4. Comparison of Mask R-CNN and Cascade R-CNN with Swin-S as the backbone. “<sup>†</sup>” indicates the results are re-produced by ours and the remaining results of PSAQ-ViT V2 [? ] and CLAMP-ViT [? ] are copied from their paper. “AP (box)” is the box AP for object detection and “AP (mask)” is the mask AP for instance segmentation.

respectively. For W4A8 Cascade R-CNN, SPDFQ achieves 0.5 and 0.2 increases on box and mask AP for W4A8 Mask R-CNN, respectively.